

## Estimation of Deformed Shapes of Beam Structures using 3D Coordinate Information from Terrestrial Laser Scanning

H.M. Lee<sup>1</sup> and H.S. Park<sup>1,2</sup>

**Abstract:** This paper presents a computational model to estimate deformed shapes of beam structures using 3D coordinate information from terrestrial laser scanning (TLS). The model is composed of five components: 1) formulation of polynomial shape function, 2) application of boundary condition, 3) inducement of compatibility condition, 4) application of the least square method and 5) evaluation of error vector and determination of reasonable polynomial shape function. In the proposed model, the optimal degree of polynomial function is selected based on the complexity of beam structures, instead of using a specific degree of polynomial function. The chosen polynomial function for estimation is forced to satisfy the boundary and compatibility conditions and allows accurate estimation of a beam structure's deformed shapes and displacement. The proposed model is experimentally applied to estimation of deformed shape of a simply supported steel beam subjected to a concentrated load. The performance of the proposed model is investigated by comparing the deflections of the beam estimated from the model and the deflections directly measured from linear variable differential transducers (LVDTs).

**Keyword:** Structural Health Monitoring, Measurement, Deflection, Deformation, Terrestrial Laser Scanning.

### 1 Introduction

Recently a number of studies have been reported on structural health monitoring techniques in building and bridge structural engineering areas. Structural health monitoring identifies and

assesses physical responses of a structure pertaining to its structural behaviors such as strain, displacement and acceleration. Such structural responses are measured from appropriate sensors and are used for assessing the structure's safety and serviceability. In particular, for a beam structure, its displacement or deflection is an important index for assessing the structure's safety and serviceability (Park et al., 2006; Park et al., 2007; Huang and Shih, 2007).

LVDTs were commonly used to measure displacements of beam structures because of its high precision level within 0.1 mm. However, since they are often difficult to install in real structures, they were mostly used for structural experiments of validation purposes in laboratories.

Displacement monitoring techniques based on GPS technology and vision-based monitoring using photogrammetry technology are being used actively. GPS-based approaches have been applied mostly on bridges and buildings (Nakamura, 2000; Xu et al., 2002; Meng et al., 2007; Park et al., 2008), and their displacement precision levels were reported as approximately 15 mm horizontally and 35 mm vertically (Nikitopoulou et al., 2006). However, GPS based monitoring has limitations in measuring structural displacements. Positions determined from GPS satellite signals are influenced by electrical cables that can cause distortion of satellite signals. Also, structural elements can impede such signals. Furthermore, displacement monitoring that requires high level precision within a few millimeters can be difficult to implement using a GPS-based approach.

Vision-based approach makes use of photogrammetry techniques that measure physical displacements using pixel digital signals of charges that are generated in proportion to the strength of op-

<sup>1</sup> Department of Architectural Engineering, Yonsei University, Seoul, 120-749, Korea

<sup>2</sup> Corresponding author, Email: hspark@yonsei.ac.kr

tical images projected to a camera through a lens. This approach usually has a precision level of approximately 1 mm in measuring not only static but also dynamic movements (Olaszek, 1999; Fraser and Riedel, 2000; Wahbeh et al., 2003). However, photogrammetry techniques for structural displacement measurements require reference targets to verify the absolute distance (Wahbeh et al., 2003) as well as multiple cameras (Fraser and Riedel, 2000). In addition, device calibration is required to ensure precision of displacement measurements by preventing image distortion from optical or electrical systems (Olaszek, 1999). Lastly, light emitting diode (LED) targets are required to enable nighttime identification.

Also, a new technique using robotic total station (RTS) is recently introduced. The technique can remotely measure the displacement of structures with accuracies of a few mm level and frequency up to 4 Hz (Psimoulis et al., 2007).

As such, each of the techniques for physical displacement monitoring, such as LVDT, GPS based technique, and vision-based monitoring, has its merits and shortcomings. They rely, however, commonly on displacement measurement of a specific portion of a structure and thus possess inherent difficulties in assessing the overall health monitoring of a structure.

Recently a laser scanning system, called Terrestrial Laser Scanning (TLS) or Light Detection And Ranging (LiDAR), has been introduced to overcome the limitations of existing measurement techniques (Park et al., 2007). TLS makes use of laser to obtain 3D coordinate information of an object remotely (Trimble, 2007; Optech, 2007) and its operation is not influenced significantly by the surroundings. It has the merit of obtaining 3D location data on the overall structure or building instead of a specific location (Ackemann, 1999). Initial applications of TLS in GIS field were performed to obtain geologic and topographic information (Kimes et al., 2006; Zhou et al., 2004; Priestnall et al., 2000). Recently TLS has been actively applied to simulation of diverse spatial phenomena (Arayici, 2007).

Park et al. (2007) used 3D coordinate information of TLS to estimate deformed shapes of a

simple beam by deriving special geometric relationships and applying the least square method. Quadratic polynomial equations were used to satisfy the conditions of deflection at the load point and continuity of slope. Compared to displacements obtained from LVDT, the TLS showed the precision level of approximately 2 mm. However, deformed shapes of a simple beam under a single concentrated load should be expressed as a polynomial of third degree or higher, in theory. Therefore, the quadratic polynomial estimation of the deformed shapes has limitations.

In this paper, to minimize errors in the estimated deformed shapes, a computational model is presented for automatic selection of the optimal degree of polynomials. The degree of a polynomial function is chosen based on the complexity of beam structures and its response instead of using a specific degree of polynomial function. The chosen polynomial function for estimation of a deformed shape is forced to satisfy the boundary and compatibility conditions of a beam structure. The performance of the proposed model is experimentally investigated.

In the following sections, a principle of 3D coordinate data extraction from TLS and the coordinate transformation method for displacement measurement are briefly described. Next, the components of computational model are presented in detail. Subsequently, the model is applied to estimation of deformed shapes and maximum deflections of a beam structure subjected to a concentrated load. Finally, the paper ends with a summary of experimental results and conclusions.

## 2 Acquisition of 3D Coordinate Data from TLS and Coordinate Transformation for Displacement Measurements

### 2.1 Principle of 3D Coordinate Data Extraction from TLS

The principle of 3D coordinate data extraction from TLS system is as shown in Figure 1. The principle of 3D coordinate data extraction from TLS is based on measuring the time it takes for the laser pulse to travel from its source to an object or structure and return, and computing the distance

based on the travel speed of the pulse. The relative coordinates of the object with respect to the laser scanner of the object with respect to the laser scanner,  $x'_i, y'_i, z'_i$  are obtained using the distance between the laser scanner and the object and the angle of the laser pulse at the time of laser pulse generation.

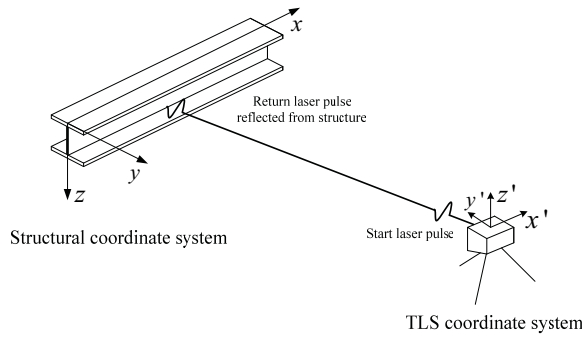


Figure 1: Principle of 3D coordinate data extraction from TLS

Here,  $i$  refers to the 3D coordinate data number obtained from the laser scanner, where  $i = 1, 2, 3, \dots, m$ .

Figure 2 shows an image based on 3D coordinates of a steel beam obtained from TLS system in accordance with the principle of Figure 1. The accuracy of 3D coordinate data of an object obtained from a TLS system depends on the type of laser scanner and the distance to the object.

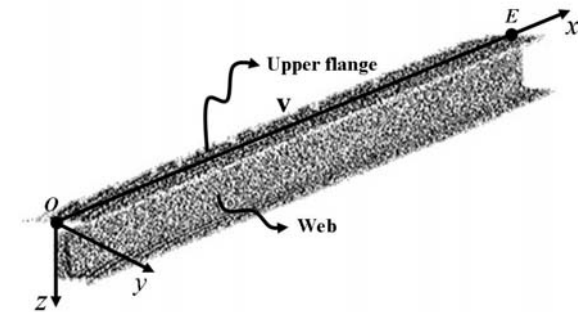


Figure 2: 3D image of the steel beam obtained from TLS

In general, TLS system can obtain 3D coordinates with precision level of about 10 mm (Trimble, 2007; Optech, 2007). The TLS system used

in this study showed directional error of about 7 mm and vertical error of about 12 mm at the measuring distance of 100 m (Trimble, 2007). However, in practice, reflection characteristics such as color, texture and angle of incidence of a laser can be caused of the errors (Stiros et al., 2007). In this study, experimental outliers of 3D coordinates from the TLS were partly shown up to about 20 mm. Such precision levels limit applicability of the technique for structural health monitoring, which requires, in general, precision level of a few millimeters. For this reason, Park et al (2007) presented a model for estimating a structure's deformed shapes using TLS 3D coordinate data.

## 2.2 Coordinate Transformation for Displacement Measurement

When 3D coordinate data are obtained on deformation of a structure from a TLS system as in Figure 1, the object's 3D coordinate data represent relative coordinates,  $x'_i, y'_i, z'_i$  based on the coordinate system  $(x', y', z')$  of the laser scanner. Therefore, 3D coordinate data obtained from TLS system cannot be used directly for measurement of a structure. The relative displacements of a structure obtained from TLS system need to be transformed to the structural coordinate system for displacement measurement. The structural coordinate system  $(x, y, z)$  must be defined in consideration of the deformation characteristics of the structure to enable the coordinate transformation.

In Figure 1, the relationship between the TLS coordinate system  $(x', y', z')$  based on the terrestrial laser scanner and the structural coordinate system  $(x, y, z)$  based on the structure's deformation characteristics, can be obtained using base vectors in consideration of the structure's shape, where the base vectors are obtained by applying the least square method and the geometric characteristics on the 3D coordinate data of the structure obtained from the laser scanner. In the case of a steel beam in Figure 2, 3D coordinates of the flange and the web areas are used where 3D coordinate information is relatively plentiful.

In Figure 2, the upper flange surface and the web surface are obtained based on the least square method, followed by the intersecting line of the

two surfaces. The intersecting point of the intersecting line and the vertical surface, which is perpendicular to the intersection line, containing the far left end point of the steel beam is the origin,  $O$ , while the intersecting point between the intersecting line and the vertical surface, which is perpendicular to the intersecting line, containing the far right end point of the steel beam on the opposite side, is the end point,  $E$ . The base vector ( $v$ ) is computed using the origin  $O$  and the end point  $E$ . The TLS coordinate system  $(x', y', z')$  can be transformed to the structural coordinate system  $(x, y, z)$ , which allows direct computation of a structure's deformation, through translation and rotation using the base vector.

### 3 Computational Model for Estimation of Deformed Shape

In section 2 it is introduced the coordinate transformation method, which transforms TLS coordinate data of a structure,  $x'_i, y'_i, z'_i$ , to the structural coordinate data,  $x_i, y_i, z_i$  which allows computation of deformed shapes. In this section computational model is presented to define polynomial shape functions suitable for various deformed shapes of beam structures from TLS 3D coordinate data,  $x_i, y_i, z_i$  of a structure. The proposed model consists of the following five components: 1) formulation of polynomial shape function, 2) application of boundary condition, 3) inducement of compatibility condition, 4) application of the least square method and 5) evaluation of error vector and determination of reasonable polynomial shape function. The five components are described below.

#### 3.1 Formulation of Polynomial Shape Function

Schematic diagram of a beam structure subjected to arbitrary loads as in Figure 3, follows differential equation of the deflection curve of Eq.1 based on Euler's beam theory.

$$\frac{d^2 z(x)}{dx^2} = \frac{M(x)}{EI} \quad (1)$$

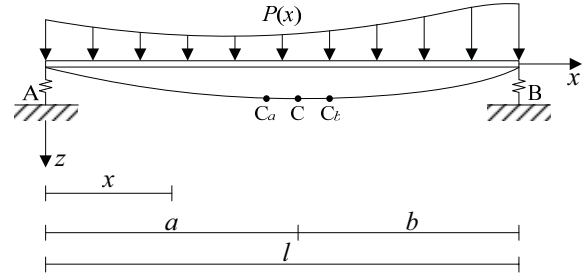


Figure 3: Schematic diagram of a beam structure subjected to arbitrary loads

Here,  $z$  is the vertical deflection,  $M$  is the bending moment,  $E$  is the modulus of elasticity and  $I$  is the second moment of inertia. From the Eq.1, deformed shape of a beam structure can be expressed as a polynomial shape function with respect to the longitudinal direction of beam depending on the load type, such as a concentrated load or distributed load, and the boundary conditions of supports. In general, it can be assumed that a beam structure's  $y$ -axis deflection, as shown in Figures 1 and 2, does not change unless its limit state are reached due to buckling. In such a case, as the first step in estimation of a deformed shape, the vertical deflection  $z(x)$  at an arbitrary point  $x$  is defined as an  $n^{\text{th}}$  polynomial function such as Eq.2.

$$z(x) = c_1 x^n + c_2 x^{n-1} + \dots + c_{n-1} x^2 + c_n x^1 + c_{n+1} \quad (2)$$

Here  $c_1, c_2, \dots, c_{n+1}$  are coefficients of the approximated function to be determined from the 3D TLS coordinate data by applying the least square method.

#### 3.2 Application of Boundary Conditions

Boundary conditions of supports can be applied for estimation of its deformed shapes from TLS 3D coordinate data. To make use of boundary conditions at two end points of a beam, two equations are needed to describe such end points. In case the beam deflection cannot be expressed in a single polynomial function because of load discontinuity, such as a concentrated load, two equations are also necessary to describe two intervals

of the beam. Boundary conditions of supports include fixed support, hinge support, roller support and spring support with variable stiffness. Boundary conditions identified for rotation and deflection at a support can be used as constraints when applying the least square method. In Figure 3, deformed shapes of the beam in intervals  $a$  and  $b$  divided at an arbitrary point,  $C$ , can be expressed by considering the boundary conditions of rotation and deflection as in Eq.3 and Eq.4.

$$z^a(x) = c_1^a x^n + c_2^a x^{n-1} + \dots + c_{n-1}^a x^2 + R_A x^1 + D_A, \quad 0 \leq x \leq a \quad (3)$$

$$z^b(x) = c_1^b (x-l)^n + c_2^b (x-l)^{n-1} + \dots + c_{n-1}^b (x-l)^2 + R_B (x-l)^1 + D_B, \quad b \leq x \leq l \quad (4)$$

In case only the initial value of beam deflection can be considered, Eq.3 and Eq.4 can be simplified as Eq.5 and Eq.6. Here, the arbitrary point  $C$  can be a position of load discontinuity or a central position of the beam.

$$z^a(x) = c_1^a x^n + c_2^a x^{n-1} + \dots + c_{n-1}^a x^2 + c_n^a x^1 + D_A, \quad 0 \leq x \leq a \quad (5)$$

$$z^b(x) = c_1^b (x-l)^n + c_2^b (x-l)^{n-1} + \dots + c_{n-1}^b (x-l)^2 + c_n^b (x-l)^1 + D_B, \quad b \leq x \leq l \quad (6)$$

Here,  $c_1^a, c_2^a, \dots, c_n^a$  and  $c_1^b, c_2^b, \dots, c_n^b$  denote coefficients of the approximated function to be defined from applying the least square method on the 3D TLS coordinate data of a structure for each interval. Also,  $R_A$  and  $R_B$  are the initial values of rotation angle at points  $A$  and  $B$  in Figure 3 while  $D_A$  and  $D_B$  denote initial values of support deflections at  $A$  and  $B$ , respectively. If boundary conditions at points are clearly defined, then the coefficients of  $R_A, R_B, D_A$ , and  $D_B$  corresponding to such boundary conditions can be determined.

### 3.3 Inducement of Compatibility Condition

Theoretically, the compatibility condition on beam continuity can be applied to a point of separation, such as  $C$  in Figure 3, or to a point of load

discontinuity. Here, unknown constants are determined to allow derivation of the beam's deflection curve equation.

However, application of the least square method to an arbitrary polynomial function of subsections 3.1 and 3.2, obtained from TLS 3D coordinate data, does not yield a definitive solution but only approximation equations are derived. Therefore, the compatibility condition is not satisfied. Furthermore, it is difficult to apply strict compatibility conditions to two or more estimated approximation equations. As an alternative, the method of deriving the compatibility approximately by incorporating mutual deformation characteristics of each beam interval is considered. When estimating an approximation expression for interval  $a$  deflection in Figure 3, the 3D coordinate data of interval  $b$  near point  $C$  (interval  $C \sim C_b$ ) are used additionally. On the other hand, the 3D coordinate data of interval  $a$  near point  $C$  (interval  $C_a \sim C$ ) are used for estimation of the approximation expression for interval  $b$ . In this way, mutual characteristics of intervals are incorporated to derive the compatibility condition in an approximate form. Consequently, Eq.3 to Eq.6 can be expressed as Eq.7 to Eq.10 with compatibility condition incorporated.

$$z^a(x) = c_1^{a'} x^n + c_2^{a'} x^{n-1} + \dots + c_{n-1}^{a'} x^2 + R_A x^1 + D_A, \quad 0 \leq x \leq C_b \quad (7)$$

$$z^b(x) = c_1^{b'} (x-l)^n + c_2^{b'} (x-l)^{n-1} + \dots + c_{n-1}^{b'} (x-l)^2 + R_B (x-l)^1 + D_B, \quad C_a \leq x \leq l \quad (8)$$

$$z^a(x) = c_1^{a'} x^n + c_2^{a'} x^{n-1} + \dots + c_{n-1}^{a'} x^2 + c_n^{a'} x^1 + D_A, \quad 0 \leq x \leq C_b \quad (9)$$

$$z^b(x) = c_1^{b'} (x-l)^n + c_2^{b'} (x-l)^{n-1} + \dots + c_{n-1}^{b'} (x-l)^2 + c_n^{b'} (x-l)^1 + D_B, \quad C_a \leq x \leq l \quad (10)$$

Here,  $c_1^{a'}, c_2^{a'}, \dots, c_n^{a'}$  and  $c_1^{b'}, c_2^{b'}, \dots, c_n^{b'}$  denote the coefficients of approximated functions to be determined from the 3D TLS coordinate data of an interval by applying the least square method.

### 3.4 Application of the Least Square Method

The least square method is an approximation method to minimize the size of error vector obtained from correlation of measured data such as from experiments. Eq.7 to Eq.10 determined in the subsections 3.1 to 3.3 can be introduced to determine the coefficients of a function that minimize the sum of squares of differences between the functional values and the measured values. When considering only the boundary conditions of deflection, Eq.9 and Eq.10 can be expressed in matrices as in Eq.11 and Eq.12.

$$\begin{Bmatrix} z_1^a \\ z_2^a \\ \vdots \\ \vdots \\ z_{m'_a}^a \end{Bmatrix} = \begin{bmatrix} x_1^n & x_1^{n-1} & \cdots & x_1^1 & 1 \\ x_2^n & x_2^{n-1} & \cdots & x_2^1 & 1 \\ \vdots & \vdots & \cdots & \vdots & \vdots \\ \vdots & \vdots & \cdots & \vdots & \vdots \\ x_{m'_a}^n & x_{m'_a}^{n-1} & \cdots & x_{m'_a}^1 & 1 \end{bmatrix} \begin{Bmatrix} c_1^{a'} \\ c_2^{a'} \\ \vdots \\ c_n^{a'} \\ D_A \end{Bmatrix} + \begin{Bmatrix} e_1^a \\ e_1^a \\ \vdots \\ \vdots \\ e_{m'_a}^a \end{Bmatrix}, \quad 0 \leq x \leq C_b \quad (11)$$

$$\begin{Bmatrix} z_1^b \\ z_2^b \\ \vdots \\ \vdots \\ z_{m'_b}^b \end{Bmatrix} = \begin{bmatrix} (x_1-l)^n & (x_1-l)^{n-1} & \cdots & (x_1-l)^1 & 1 \\ (x_2-l)^n & (x_2-l)^{n-1} & \cdots & (x_2-l)^1 & 1 \\ \vdots & \vdots & \cdots & \vdots & \vdots \\ \vdots & \vdots & \cdots & \vdots & \vdots \\ (x_{m'_b}-l)^n & (x_{m'_b}-l)^{n-1} & \cdots & (x_{m'_b}-l)^1 & 1 \end{bmatrix} \begin{Bmatrix} c_1^{b'} \\ c_2^{b'} \\ \vdots \\ c_n^{b'} \\ D_B \end{Bmatrix} + \begin{Bmatrix} e_1^b \\ e_1^b \\ \vdots \\ \vdots \\ e_{m'_b}^b \end{Bmatrix}, \quad C_a \leq x \leq l \quad (12)$$

Here,  $m'_a, m'_b$  denote the sum of the number of coordinate data of intervals  $a$  and  $b$  plus the num-

ber of coordinate data of interval  $C \sim C_b$ , interval  $C_a \sim C$ , respectively. Also,  $e_1^a, e_2^a, \dots, e_{m'_a}^a, e_1^b, e_2^b, \dots, e_{m'_b}^b$  denote errors between the assumed polynomial function and coordinate data obtained from TLS. Eq.11 and Eq.12 are expressed in matrix vector form as follows.

$$\mathbf{z}_a = \mathbf{X}_a \boldsymbol{\xi}_a + \mathbf{e}_a, \quad 0 \leq x \leq C_b \quad (13)$$

$$\mathbf{z}_b = \mathbf{X}_b \boldsymbol{\xi}_b + \mathbf{e}_b, \quad C_a \leq x \leq l \quad (14)$$

Therefore, the error vectors are expressed as follows.

$$\mathbf{e}_a = \mathbf{z}_a - \mathbf{X}_a \boldsymbol{\xi}_a, \quad 0 \leq x \leq C_b \quad (15)$$

$$\mathbf{e}_b = \mathbf{z}_b - \mathbf{X}_b \boldsymbol{\xi}_b, \quad C_a \leq x \leq l \quad (16)$$

The unknown  $\boldsymbol{\xi}$  vector can be computed as follows from minimization of the sum of squares of  $\mathbf{e}$  vector elements.

$$\boldsymbol{\xi}_a^* = (\mathbf{X}_a^T \mathbf{X}_a)^{-1} \mathbf{X}_a^T \mathbf{z}_a, \quad 0 \leq x \leq C_b \quad (17)$$

$$\boldsymbol{\xi}_b^* = (\mathbf{X}_b^T \mathbf{X}_b)^{-1} \mathbf{X}_b^T \mathbf{z}_b, \quad C_a \leq x \leq l \quad (18)$$

### 3.5 Evaluation of Error Vectors and Determination of Reasonable Polynomial Shape Function

As described in the subsections 3.1 to 3.3, it is introduced an arbitrary  $n^{th}$  polynomial function in consideration of support's boundary conditions and compatibility condition. To this polynomial function, enter the 3D TLS coordinate data and apply the least square method as in Eq.17 and Eq.18. Then, the error vectors  $\mathbf{e}_a^*$  and  $\mathbf{e}_b^*$  are computed as in Eq.19 and Eq.20 on the deformed shapes determined from the least square method and the 3D TLS coordinate data.

$$\mathbf{e}_a^* = \mathbf{z}_a - \mathbf{X}_a \boldsymbol{\xi}_a^*, \quad 0 \leq x \leq C \quad (19)$$

$$\mathbf{e}_b^* = \mathbf{z}_b - \mathbf{X}_b \boldsymbol{\xi}_b^*, \quad C \leq x \leq l \quad (20)$$

Next, using the number of coordinate data of each interval, the precision levels,  $\sigma_a^*$  and  $\sigma_b^*$  for error evaluation are determined as in Eq.21 and Eq.22. From Eq.21 and Eq.22, the precision levels for various polynomial functions (2<sup>nd</sup>-5<sup>th</sup>, table 1)

are evaluated, and then the coefficient vectors,  $\xi^a$  and  $\xi^b$  having the minimum error are determined.

$$\sigma_a^* = \frac{\|\mathbf{e}_a^*\|}{\sqrt{m_a}} \quad (21)$$

$$\sigma_b^* = \frac{\|\mathbf{e}_b^*\|}{\sqrt{m_b}} \quad (22)$$

Thus, the deformed shape equations Eq.23 and Eq.24 can be obtained from the coefficient vectors  $\xi^a$  and  $\xi^b$  and the longitudinal position vectors  $\mathbf{x}^a$  and  $\mathbf{x}^b$ .

$$\mathbf{z}^a(x) = \xi^{aT} \mathbf{x}_a, \quad 0 \leq x \leq C \quad (23)$$

$$\mathbf{z}^b(x) = \xi^{bT} \mathbf{x}_b, \quad C \leq x \leq l \quad (24)$$

### 3.6 Computational Procedure

This subsection describes the algorithm for applying the proposed model in steps. The application algorithm consists of eight steps as follows.

**Step 1.** Input 3D coordinate data:  $x_i, y_i, z_i$ .

**Step 2.** Set initial conditions.

- 1) Boundary conditions of supports:  $R_A, R_B, D_A, D_B$ .
- 2) Degree of polynomial function:  $n_{\min}, n_{\max}$ .
- 3) Separation point:  $C$ .
- 4) Boundaries for compatibility conditions:  $C_a, C_b$ .

**Step 3.** Formulate polynomial function matrix: Eq.13 and Eq.14.

**Step 4.** Apply the least square method: Eq.17 and Eq.18.

**Step 5.** Determine precision levels: Eq.21 and Eq.22.

**Step 6.** Repeat Step 3 ~ Step 5.

**Step 7.** Determine coefficients of polynomial functions:  $\xi^a, \xi^b$ .

**Step 8.** Estimate deformed shapes and displacement: Eq.23 and Eq.24.

## 4 Application of Computational Model

### 4.1 Experimental Setup

To evaluate the performance of the proposed model, a bending test of a simply supported steel beam subjected to a point load at the mid-span is conducted as in Figure 4 and Figure 5. The beam is a Korean H-section with a depth of 100 mm, flange width of 100 mm, web thickness of 6 mm, and flange thickness of 6 mm. The grade of steel for the beam is a Korean SS400 with specified yield strength of  $F_y = 253.3\text{MPa}$ . The beam is designed to generate pure bending along the beam length direction. At the mid-span,  $l/2$  of the steel beam, loads of 4.95 ( $P_1$ ), 9.66 kN ( $P_2$ ), 14.88 kN ( $P_3$ ) are applied sequentially, and TLS and LVDTs are used for each load to obtain the 3D coordinates of the beam and its deflection at locations of  $l/8, l/4, 3l/8, l/2, 5l/8, 3l/4$  and  $7l/8$  as in Figure 5.

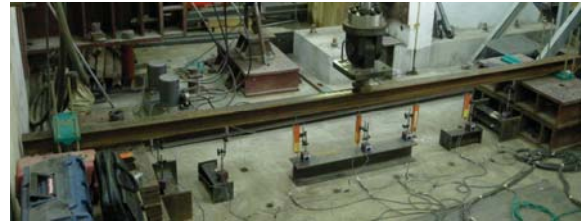


Figure 4: Experimental setup

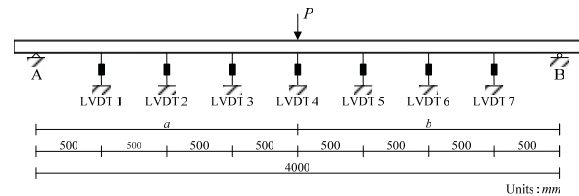


Figure 5: Schematic diagram of the experiment setup

### 4.2 Application of Computational Model

The 3D coordinate data of the beam were obtained from TLS at approximately 3 m from the experiment set as in Figure 6. Figure 7 shows images of the steel beam before and after application of

Table 1: Vertical deflections of the beam from LVDTs and TLS computational model

Loading step	Measuring techniques	Deflections (mm)									
		$l/8$	$l/4$	$3l/8$	$l/2$ (a)	$l/2$ (b)	$5l/8$	$3l/4$	$7l/8$	$\sigma_a^*$	$\sigma_b^*$
$P_1 = 4.95$ kN	LVDT	-3.08	-5.73	-7.59	-8.35	-8.35	-7.58	-5.84	-3.17	-	-
	TLS_2nd	-3.13	-5.55	-7.23	-8.14	-8.30	-7.11	-5.61	-3.37	0.92	0.95
	TLS_3rd	-2.91	-5.54	-7.41	-8.05	-8.14	-7.41	-5.57	-2.98	0.91	0.92
	TLS_4th	-2.86	-5.61	-7.39	-8.02	-8.13	-7.41	-5.59	-2.96	0.91	0.92
	TLS_5th	-2.87	-5.62	-7.37	-8.06	-8.15	-7.39	-5.60	-2.97	0.91	0.92
$P_2 = 9.66$ kN	LVDT	-6.05	-11.22	-14.79	-16.29	-16.29	-14.75	-11.40	-6.26	-	-
	TLS_2nd	-6.21	-11.01	-14.36	-16.24	-16.32	-14.24	-11.10	-6.49	0.96	1.01
	TLS_3rd	-5.83	-10.99	-14.67	-16.07	-16.14	-14.61	-11.06	-6.01	0.93	0.96
	TLS_4th	-5.82	-10.99	-14.67	-16.06	-16.14	-14.61	-11.06	-6.01	0.93	0.96
	TLS_5th	-5.83	-11.01	-14.64	-16.12	-16.12	-14.62	-11.05	-6.00	0.93	0.96
$P_3 = 14.88$ kN	LVDT	-9.20	-17.03	-22.57	-24.79	-24.79	-22.52	-17.33	-9.51	-	-
	TLS_2nd	-9.62	-16.93	-21.92	-24.54	-24.65	-21.87	-17.11	-9.96	1.03	1.03
	TLS_3rd	-9.19	-16.92	-22.28	-24.34	-24.40	-22.34	-17.05	-9.34	1.00	0.95
	TLS_4th	-9.22	-16.87	-22.29	-24.36	-24.39	-22.33	-17.08	-9.32	1.00	0.95
	TLS_5th	-9.23	-16.88	-22.27	-24.41	-24.36	-22.35	-17.07	-9.31	1.00	0.95

Table 2: Vertical deflection errors of TLS computational model based on the LVDT

Loading step	Degree of polynomials	Deflection errors (mm)									
		$l/8$	$l/4$	$3l/8$	$l/2$ (a)	$l/2$ (b)	$5l/8$	$3l/4$	$7l/8$	$\sigma_a$	$\sigma_b$
$P_1 = 4.95$ kN	TLS_2nd	0.05	-0.17	-0.35	-0.21	-0.05	-0.47	-0.24	0.20	0.23	0.28
	TLS_3rd	-0.17	-0.19	-0.18	-0.30	-0.21	-0.17	-0.27	-0.19	0.22	0.22
	TLS_4th	-0.23	-0.12	-0.19	-0.34	-0.22	-0.18	-0.25	-0.21	0.23	0.22
	TLS_5th	-0.22	-0.11	-0.22	-0.30	-0.20	-0.19	-0.24	-0.20	0.22	0.21
$P_2 = 9.66$ kN	TLS_2nd	0.16	-0.21	-0.43	-0.06	0.03	-0.51	-0.30	0.24	0.25	0.32
	TLS_3rd	-0.23	-0.23	-0.11	-0.23	-0.15	-0.13	-0.34	-0.25	0.20	0.24
	TLS_4th	-0.23	-0.22	-0.12	-0.23	-0.15	-0.13	-0.34	-0.25	0.21	0.24
	TLS_5th	-0.22	-0.21	-0.15	-0.18	-0.17	-0.12	-0.35	-0.25	0.19	0.24
$P_3 = 14.88$ kN	TLS_2nd	0.42	-0.10	-0.65	-0.25	-0.14	-0.65	-0.22	0.45	0.41	0.42
	TLS_3rd	-0.01	-0.11	-0.28	-0.45	-0.39	-0.18	-0.28	-0.17	0.27	0.27
	TLS_4th	0.03	-0.16	-0.27	-0.43	-0.40	-0.18	-0.25	-0.19	0.27	0.27
	TLS_5th	0.04	-0.15	-0.30	-0.38	-0.43	-0.17	-0.26	-0.20	0.26	0.28

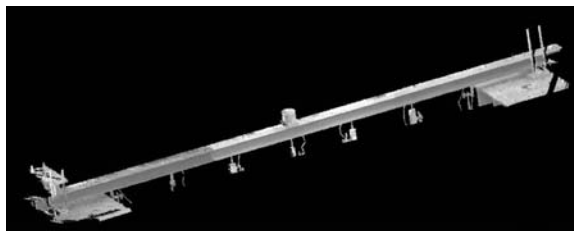


Figure 6: 3D image of the steel beam obtained from TLS

the loadings. Approximately 40,000 and 20,000 3D coordinate data points were obtained from the web and the upper flange of the steel beam, respectively. The 3D coordinate data from the web and the upper flange of Figure 7(a) were used for coordinate transformation from TLS coordinate system to the structural coordinate system. Also, the 3D coordinate data of the upper flange, which represent the deformation characteristics of the steel beam effectively, were used for the deformation computation model.

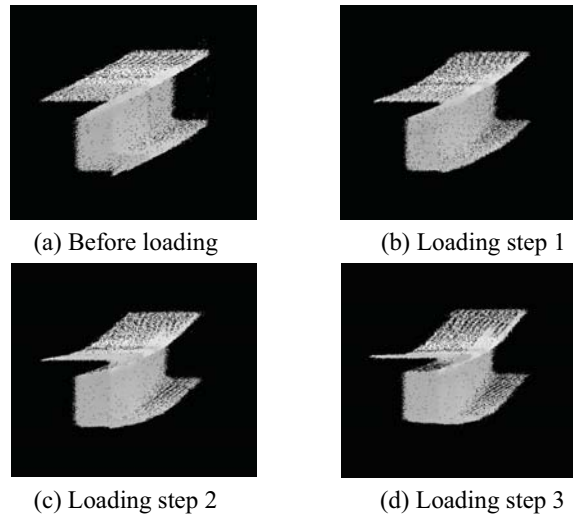


Figure 7: 3D images of the steel beam before and after loading

Thus, the 3D coordinate data of the upper flange (Figures 7(b), (c) and (d)) based on the three different loads of 4.95 kN ( $P_1$ ), 9.66 kN ( $P_2$ ), 14.88 kN ( $P_3$ ) obtained from TLS are applied coordinate transformation to obtain the 3D coordinate input data for displacement measurement. For the initial condition setting, 0 is entered for the boundary conditions  $D_A$  and  $D_B$  for vertical deflection in Eq.9 and Eq.10. The degrees of the polynomial function were considered minimum degree of 2 to maximum degree of 5 based on Euler's beam theory. The mid-span of the beam is set as separation point which divides the equations due to the load discontinuity. Boundaries for deriving the compatibility condition are set as 1,800 mm and 2,200 mm from location A in Figure 5 considered 1/10 of each interval. Then, polynomial matrices are formed in consideration of configured boundary conditions and compatibility conditions. Based on the initial configured degree of the polynomials, Step 3 to Step 5 in the subsection 3.6 are repeated to obtain coefficient vectors of the polynomials and the precision level of each coefficient vector is evaluated. Finally, the coefficient vectors of the polynomials are determined based on the precision evaluation and the beam deformed shapes are estimated.

## 5 Results and Discussion

### 5.1 Determination of Polynomial Function

From Steps 1~8 in the subsection 3.6, deformed shapes of the steel beam were determined for each load of 4.95 kN ( $P_1$ ), 9.66 kN ( $P_2$ ), 14.88 kN ( $P_3$ ). Figure 8 shows histograms of errors between the 3D coordinate data and the estimated deformed shapes. The error distribution in Figure 8 shows a standard normal distribution. Polynomials of degree 2 to 5 except in cases of quadratic polynomials in Figures 8 (a), (e) and (i), show similar histograms for each load. This implies that the estimated deformed shapes converge to specific solutions with respect to the 3D coordinate data.

Estimated vertical deflections per polynomials of degree 2 to 5 and the deflections directly measured from LVDTs for each load are as in Table 1. In this table,  $\sigma_a^*$ ,  $\sigma_b^*$  denote the standard deviations computed from Eq.21 and Eq.22 for each polynomial expression. In Table 1, in case of using a quadratic polynomial for the load of 4.95 kN ( $P_1$ ), the standard deviation of interval  $a$  was computed as 0.92 mm and that for interval  $b$  was 0.95 mm. When applying a cubic polynomial for the load of 4.95 kN ( $P_1$ ), the standard deviation of interval  $a$  was computed as 0.91 mm and that for interval  $b$  was 0.92 mm, showing improvement of precision level relative to the case of a quadratic polynomial. The results of applying polynomials of degree 4 and degree 5 were similar to the results of a cubic polynomial with a standard error of 0.002 mm. Figure 9(a) shows the standard deviation of 3D coordinate data based on the deformed shapes estimated from 3D coordinate data for degree 2 to 5 per each load. Here, the standard deviation converges uniformly from polynomials of degree 3 and higher. Table 2 shows errors of vertical deflections estimated from the model compared to deflections directly measured from LVDTs. In Table 2,  $\sigma_a$  and  $\sigma_b$  denote the standard deviations of estimated vertical deflections from TLS model based on the LVDTs. Similarly, the standard deviation converges uniformly from polynomials of degree 3 and higher (Figure 9(b)). From the tables and figures in the previous section, polynomials of degree 3 are predicted to be

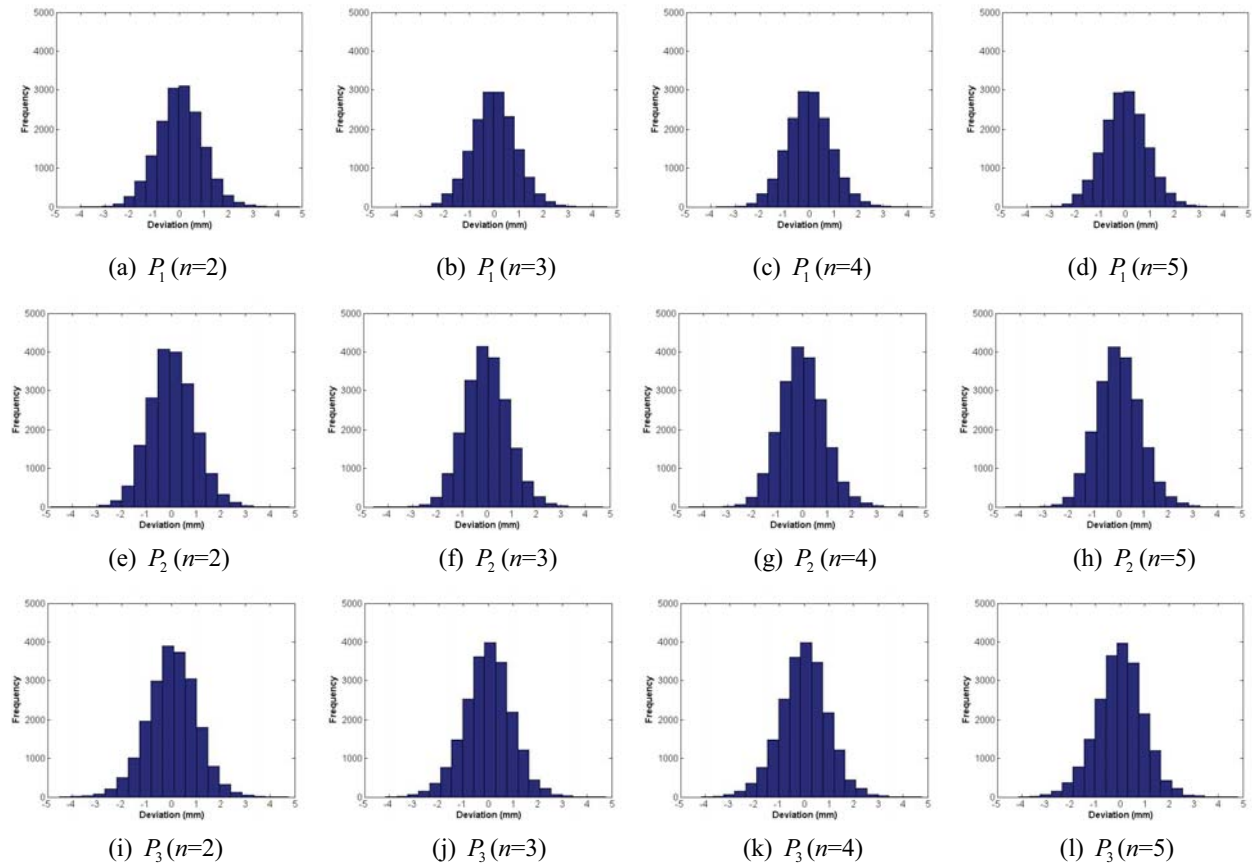


Figure 8: 3D image of the steel beam obtained from TLS

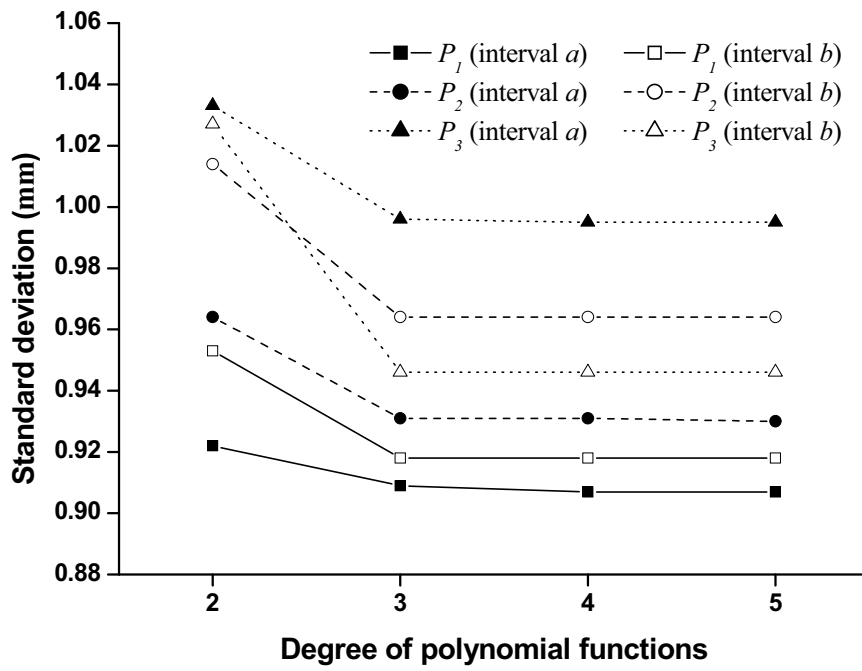
the minimum degree polynomials suitable for estimating deformed shapes of a target experiment set. According to Euler's beam theory, the vertical deflection of a simple beam under a concentrated load can be expressed as a cubic polynomial. And this fact was verified from our experiment results and the proposed deformation computational model can be used to determine the polynomial expressions for accurate prediction of the beam's deformed shape.

## 5.2 Accuracy

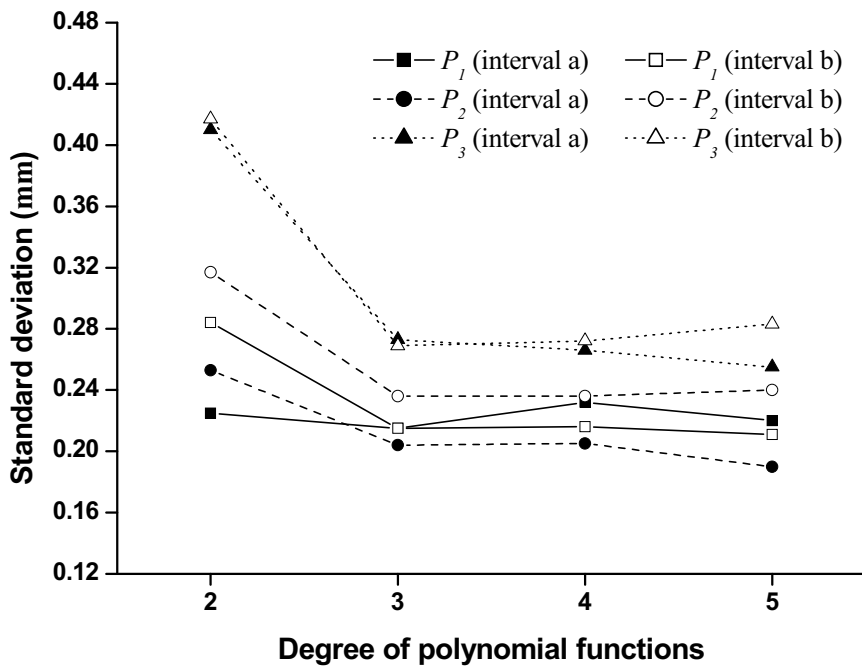
In the subsection 5.1 cubic polynomials were verified to be the minimum degree polynomials suitable for estimating the deformed shapes of a target structure. In this subsection, the accuracy of the deformed shapes estimated from quadratic polynomials and cubic polynomials from the proposed model is analyzed relative to the vertical deflections measured directly using LVDTs. Fig-

ure 10(a) and (b) show the beam deflections from LVDTs and the computational model when applying quadratic and cubic polynomials for different load levels, while Figure 11(a) and (b) show the deflection errors of the same.

When computing deformation from quadratic polynomials (Figure 11(a) and Table 2), the maximum error occurred at position as  $-0.47$  mm ( $P_1$ ),  $-0.51$  mm ( $P_2$ ), and  $-0.65$  mm ( $P_3$ ). When using cubic polynomials (Figure 11(b) and Table 2), the maximum error occurred at position  $3/4$  or position  $1/2$  as  $-0.27$  mm ( $P_1$ ),  $-0.34$  mm ( $P_2$ ), and  $-0.42$  mm ( $P_3$ ). The amplitude of deflection error was the greatest between positions  $5/8$  and  $7/8$  in Figure 11(a) as  $1.10$  mm ( $P_3$ ) while that in Figure 11(b) was the difference between position  $1/8$  and position  $1/2$  as  $0.41$  mm ( $P_3$ ). In Figure 11(a) the deflection error based on LVDTs shows a symmetric pattern centered on the beam's center with amplitude of  $1$  mm or greater. In Figure

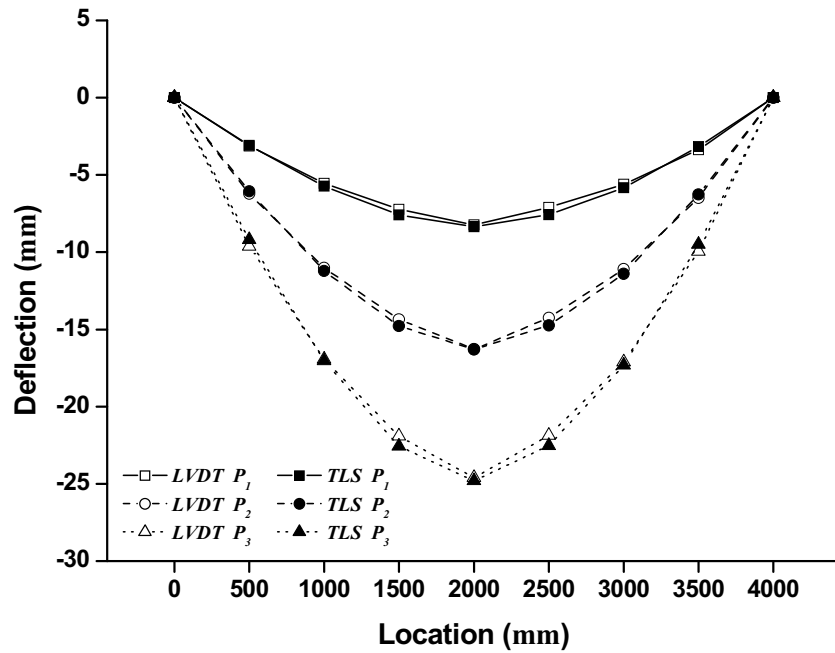


(a) Standard deviations of 3D coordinate data based on the TLS model

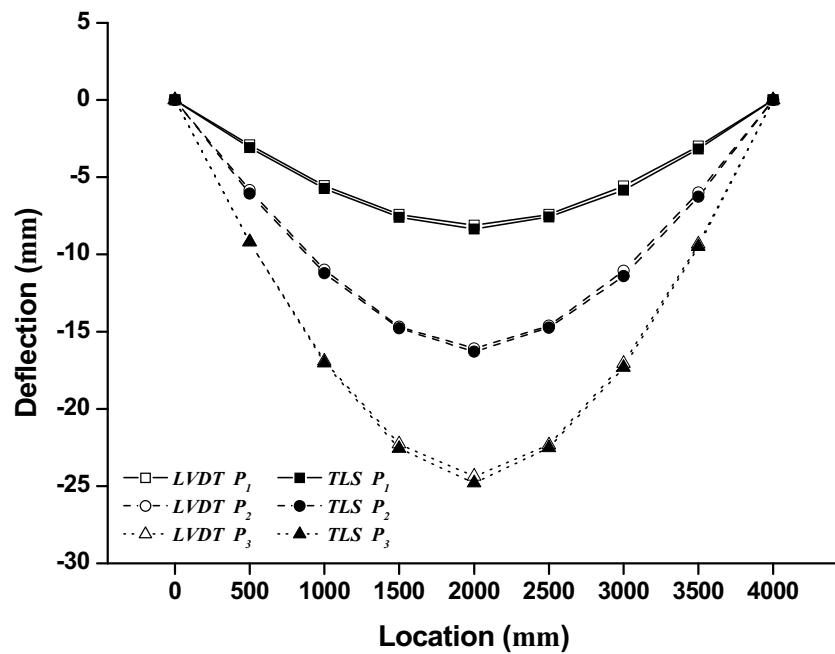


(b) Standard deviations of estimated deflections from TLS model based on the LVDT

Figure 9: Standard deviation for different degrees of deformed shapes estimated from 3D coordinate data

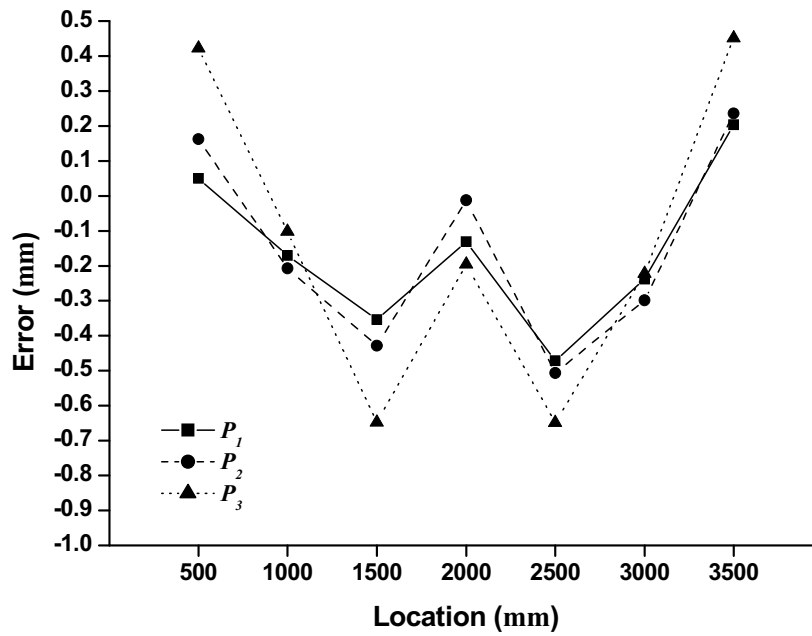


(a) Quadratic polynomial

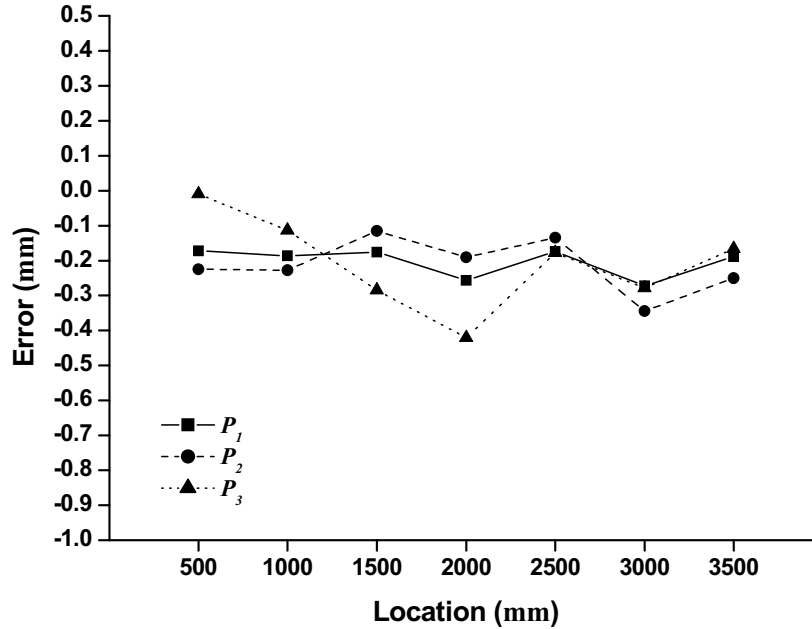


(b) Cubic polynomial

Figure 10: Vertical deflections for each load level from LVDTs and TLS computational model when applying quadratic and cubic polynomials



(a) Quadratic polynomial



(b) Cubic polynomial

Figure 11: Vertical deflection errors for each load level of TLS computational model based LVDT when applying quadratic and cubic polynomials

11(b) the same varies irregularly with amplitude of 0.5 mm or less. From these results it can be deduced that the deformed shapes estimation using quadratic polynomials does not properly reflect the deformation pattern of steel beams under concentrated loads relative to that estimated from cubic polynomials. Furthermore, it is noted that the accuracy of the deformation pattern estimated using cubic polynomials determined from the proposed model falls within 0.5 mm of the vertical deflections measured directly using LVDTs.

### 5.3 Compatibility

In each interval (interval  $a$  and interval  $b$  in Figure 5) the coordinate data of the opposite interval was included approximately 10 percent to incorporate the mutual characteristics and derive the compatibility conditions. To verify results of compatibility conditions, the errors of each interval were compared at the continuity point ( $l/2$ ) of each interval. Prior to deriving compatibility conditions, the vertical deflection error at  $l/2$  position in interval  $a$  and interval  $b$  was the maximum as 0.29 mm when applying quadratic polynomials for load  $P_1$ . The average error of polynomials of degree 2~5 for loads  $P_1$ ,  $P_2$ , and  $P_3$  was 0.15 mm. After inducement of the compatibility condition, the vertical deflection error at  $l/2$  position in interval  $a$  and interval  $b$  was maximum as 0.16 mm when applying quadratic polynomials for load  $P_1$  while the average error of polynomials of degree 2~5 for loads  $P_1$ ,  $P_2$ , and  $P_3$  was 0.07 mm. Therefore, it is noted that the error was reduced to less than half of what it was prior to deriving the compatibility condition. In this paper approximately 10 percent of the opposite interval's coordinate data was included to derive the compatibility condition. Here, it is observed that the amount of the opposite interval's data can be modified appropriately depending on the deflection pattern of two intervals  $a$  and  $b$ .

### 5.4 Comments on Practical Applications

This research intends to advance the application of TLS for health monitoring of structural safety and serviceability. The safety and serviceability of a structure or a structural member can be as-

essed by monitoring both the deformed shape and the maximum values of displacements. The displacement measurement model using TLS can be applied to periodic monitoring of the structural responses of existing buildings and bridges.

For practical applications, deflection accuracy in the order of millimeters is required in health monitoring of structures. Use of the displacement measurement model in a laboratory environment allows very precise measurements of displacements of a steel beam with the idealized experimental setup. However, for practical application of the model to actual structures in field, further investigation on various factors affecting the precision of displacement measurement such as the measuring scheme, the distance of the scanner from the surveyed object, the surface conditions of targets with different reflection characteristics (Stiros et al, 2007) are required.

## 6 Conclusions

This paper presented a model for estimating deformed shapes and displacements of a structure for structural health monitoring using TLS. The proposed model consists of the following five components: 1) formulation of polynomial shape function, 2) application of boundary conditions, 3) inducement of compatibility conditions, 4) application of the least square method and 5) evaluation of error vector and determination of reasonable polynomial shape function. The model provides a methodology for actively estimating deformed shapes of a beam structure from 3D coordinate data obtained from TLS.

The proposed model was applied on a simply supported steel beam subjected to a concentrated load to estimate the structure's deformed shapes. The performance of the model was assessed for a number of parameters based on LVDT measurements. From such results, the following conclusions are made.

- (1) In the proposed model, the optimal degree of polynomial function is selected based on the complexity of beam structures, instead of using a specific degree of polynomial function. The chosen polynomial function for

estimation is forced to satisfy the boundary and compatibility conditions and allows accurate estimation of a beam structure's deformed shapes and displacement.

- (2) When estimating deformed shapes of a structure, support boundary conditions such as fixed support, roller support, hinge support and spring support can be considered. Boundary conditions obtained from other measurement devices, such as LVDT and inclinometer which allow partial sensing, can also be considered as necessary for this purpose.
- (3) A method for satisfying continuity compatibility condition was presented to resolve the interval discontinuity problem of the deformed shapes being estimated.
- (4) The model allows estimation of a beam structure's deformed shapes within the precision level of 0.5 mm. Such estimated deformed shapes provide indices of a structure's serviceability and the corresponding displacement load provides a measure for the structure's safety assessment.

**Acknowledgement:** The work presented in this paper was supported by the National Research Laboratory Program (Project No. 2005-01504) of the Ministry of Science and Technology of Korea.

#### References:

- Ackemann, F.** (1999): Airborne laser scanning-present status and future expectation. *ISPRS Journal of Photogrammetry and Remote Sensing*, 54: 64-67.
- Arayici, Y.** (2007): An approach for real world data modeling with the 3D terrestrial laser scanner for built environment. *Automation in Construction*, 16: 816-829.
- Fraser, C.S.; Riedel, B.** (2000): Monitoring the thermal deformation of steel beams via vision metrology. *ISPRS Journal of Photogrammetry and Remote Sensing*, 55: 268-276.
- Huang, C.H.; Shih, C.C.** (2007): An inverse problem in estimating simultaneously the time-dependent applied force and moment of an Euler-Bernoulli beam. *CMES: Computer Modeling in Engineering & Science.*, 21: 239-254.
- Kimes, D.S.; Ranson, K.J.; Sun, G.; Blair, J.B.** (2006): Predicting LIDAR measured forest vertical structure from multi-angle spectra data. *Remote Sensing of Environment*, 100: 503-511.
- Meng, X.; Dodson, A.H.; Roberts, G.W.** (2007): Detecting bridge dynamics with GPS and triaxial accelerometers. *Engineering Structures*, 29: 3178-3184.
- Nakamura, S.** (2000): GPS measurement of wind-induced suspension bridge girder displacements. *Journal of Structure Engineering*, 126(12): 1413-1419.
- Nickitopoulou, A.; Protopsalti, K.; Stiros, S.** (2006): Monitoring dynamic and quasi-static deformation of large flexible engineering structures with GPS: Accuracy, limitations and promises. *Engineering Structures*, 28: 1471-1482.
- Olaszek, P.** (1999): Investigation of the dynamic characteristic of bridge structures using a computer vision method. *Measurement*, 25: 227-236.
- Optech.** (2007): Optech ILRIS-3D Scanner Brochure. from: <http://www.optech.ca/>.
- Park, H.S.; Jung, H.S.; Kwon, Y.H.; Seo, J.H.** (2006): Mathematical models for assessment of the safety of steel beams based on average strains from long gage optic sensors. *Sensors and Actuators A*, 125: 109-113.
- Park, H.S.; Jung, S.M.; Lee, H.M.; Kwon, Y.H.; Seo, J.H.** (2007): Analytical models for assessment of the safety of multi-span steel beams based on average strains from long gage optic sensors. *Sensors and Actuators A*, 137: 6-12.
- Park, H.S.; Lee, H.M.; Adeli, H.; Lee, I.** (2007): A new approach for health monitoring of structures: Terrestrial laser scanning. *Computer-Aided Civil and Infrastructure Engineering*, 22: 19-30.
- Park, H.S.; Shon, H.G.; Kim, I.S.; Park, J.H.** (2008): Application of GPS to monitoring of wind-induced responses of high-rise buildings. *Struct. Design Tall Spec. Build.*, 17: 117-132.
- Priestnall, G.; Jaafar, J.; Duncan A.** (2000): Extracting urban features from LiDAR digital sur-

face models. *Computer, Environment and Urban Systems*, 24: 65-78.

**Psimoulis, P.A.; Stiros, S.C.** (2007): Measurement of deflections and of oscillation frequencies of engineering structures using Robotic Theodolites (RTS). *Engineering Structures*, 29: 3312-3324.

**Stiros, S.; Lontou, P.; Voutsina, A.; Psimoulis, P.; Kontogianni, V.; Pytharouli, S.** (2007): Tolerance of a laser reflectorless EDM instrument. *Survey Review*, 39: 308-315.

**Trimble.** (2007): Trimble GX 3D Scanner Brochure. from: <http://www.trimble.com/>.

**Wahbeh, A.M.; Caffrey, J.P.; Masri, S.F.** (2003): A vision-based approach for the direct measurement of displacements in vibrating systems. *Smart Material and Structures*, 12: 785-794.

**Xu, L.; Guo, J.; Jiang, J.** (2002): Time-frequency analysis of a suspension bridge based on GPS. *Journal of Sound Vibration*, 254: 105-116.

**Zhou, G.; Song, C.; Simmers, J.; Cheng, P.** (2004): Urban 3D GIS From LiDAR and digital aerial images. *Computers & Geosciences*, 30: 345-353.